

## Article

# Study on Multi-Scale Coral Reef Pore Structure Identification and Characterization

Jinchao Wang <sup>1,2,\*</sup> , Qijun Guo <sup>3</sup>, Wei Chen <sup>2,4</sup> and Houceng Liu <sup>3</sup>

<sup>1</sup> State Key Laboratory of Geomechanics and Geotechnical Engineering, Institute of Rock and Soil Mechanics, Chinese Academy of Sciences, Wuhan 430071, China

<sup>2</sup> Key Laboratory of Carbonate Reservoirs, CNPC, Hangzhou 310023, China; journalarticleswh@163.com

<sup>3</sup> Institute of Rock and Soil Mechanics, Chinese Academy of Sciences, Wuhan 430071, China; whrmscientific@163.com (Q.G.); rockwhrsmmpaper@163.com (H.L.)

<sup>4</sup> PetroChina Hangzhou Research Institute of Geology, Hangzhou 310023, China

\* Correspondence: jcwang@whrsm.ac.cn

**Abstract:** In order to more accurately realize the automatic identification and quantitative characterization of coral reef multi-scale pore structure, this paper has carried out such research. On the basis of using multiple information acquisition technology, it can effectively collect field measured data and indoor observation data to form a high-precision digital image of the development characteristics of multi-scale coral reef pore structure. By constructing the multi-scale structure information correlation and fusion function of coral reef pore structure, it can formulate the positioning and search strategy for the key areas of coral reef pore structure development characteristics. In this paper, a fine identification and quantitative characterization method suitable for the pore structure of “millimeter–micron–nanometer” is formed. At the same time, combined with the actual project requirements, the multi-scale pore structure feature area location method of coral reef is constructed, which combines the distribution characteristics, variation characteristics, fractal characteristics and shape characteristics in a certain range, and realizes the search of pore key areas between different scales and different regions of the same scale through the similarity matching algorithm, which can effectively realize the automatic search of key areas in the “millimeter–micron–nanometer”-scale image of coral reefs. Finally, the correctness and feasibility of this method are verified by multi-angle example data comparison. It shows that this method can effectively solve the productivity prediction and evaluation problem of coral reef oil and gas reservoirs.

**Keywords:** coral reefs; multi-scale structure; digital image; automatic identification; quantitative characterization; feature search



**Citation:** Wang, J.; Guo, Q.; Chen, W.; Liu, H. Study on Multi-Scale Coral Reef Pore Structure Identification and Characterization. *Appl. Sci.* **2022**, *12*, 5280. <https://doi.org/10.3390/app12105280>

Academic Editor: Arcady Dyskin

Received: 21 April 2022

Accepted: 20 May 2022

Published: 23 May 2022

**Publisher's Note:** MDPI stays neutral with regard to jurisdictional claims in published maps and institutional affiliations.



**Copyright:** © 2022 by the authors. Licensee MDPI, Basel, Switzerland. This article is an open access article distributed under the terms and conditions of the Creative Commons Attribution (CC BY) license (<https://creativecommons.org/licenses/by/4.0/>).

## 1. Introduction

In today's world, the ocean has become one of the main fields of international competition. Marine resources are an important foundation and guarantee for human social and economic development. The scale of marine resources occupied and controlled by a country largely determines its marine economic development level, and even the economic and welfare level of the whole country [1,2]. As a part of the marine environment and resources, coral reefs are the most diverse communities in the sea, probably with 1–9 million species, most of which are undescribed [3]. Although their area accounts for only 0.2% of the world's marine ecosystems, their value and services account for 2.85% of the world's marine ecosystems [4], which shows the contribution of coral reefs to the world. Coral reef is a special type of rock and soil. It refers to the rock mass composed of the remains of reef coral groups after death. Its main body is coral (a coelenterate in the ocean). During its growth, coral absorbs calcium and carbon dioxide in seawater, secretes calcium carbonate and becomes its own survival shell. Coral reefs are extremely valuable land resources in tropical and subtropical oceans. They have become the foothold for marine development

and the protection of marine rights and interests. They can be built into the support and front base for modern deep-sea pelagic fisheries, marine energy development, seabed oil and gas resource development, tourism, transportation and national defense. Scientific research on coral reefs has extremely important strategic significance, scientific significance and economic value [5,6].

As a new field of global oil and gas resources development, marine oil and gas resources have become an important replacement area of global oil and gas resources [7–9]. Coral reef is a marine carbonate rock composed of reef building corals through diagenesis. The pores are relatively developed, with good permeability and a high abundance of organic matter. It is an ideal oil and gas reservoir [10]. In the study of coral reef skeleton limestone, pore structure is an important parameter affecting the physical, mechanical and chemical properties of reservoir rocks. Pore shape and pore size distribution have a great impact on oil and gas migration and reservoir capacity. Because the pores of coral reefs are the main reservoir space, determining the scale, structure and distribution characteristics of pores can contribute to scientific and reasonable stratigraphic division and reservoir evaluation, which can provide basic data for the efficient development of coral reefs as oil and gas reservoirs. The strong heterogeneity of coral reef pores and the complex diagenetic process of reef limestone led to a large number of irregular pore characteristics in coral reef strata. The core of coral reef reservoir interpretation and evaluation is to determine its pore space characteristics and master the development characteristics of coral reef pore structure, which is of great significance for reservoir evaluation [11]. The key problem of oil and gas reservoir exploration and development is the structural characterization and morphological description of reservoir space. The development characteristics of coral reef pore structure are diverse, complex and heterogeneous, which makes the quantitative characterization of coral reef pore structure very challenging.

At present, there are obvious differences in the characterization methods for stone bulk density determinations (for example water and mercury displacement method) and for direct and indirect measurements of rock porosity in different scales of coral reef. In the macroscale structure analysis and characterization of coral reef pore structure, engineering logging or direct observation are mainly used. In the microscale structure analysis and characterization of coral reef pore structure, the high-precision measuring instruments in the laboratory are mainly used. At the same time, there are few studies on the combination of macroscale structure characterization and microscale structure characterization, and considering mesoscopic-scale structure characterization. Because the different scale structure characteristics of coral reef pores have a certain correlation, in order to more accurately realize the quantitative characterization of coral reef multi-scale pore structure, this project has carried out the research on the identification and characterization method of coral reef multi-scale pore structure. By using multiple information acquisition technology, effectively collecting field measured data and indoor observation data, and forming a high-precision digital image of multi-scale coral reef pore structure development characteristics, a unified identification and characterization method of coral reef multi-scale pore structure is constructed, combined with the positioning and search strategy of key areas of coral reef pore structure development characteristics, which realize the correlation and fusion of macroscale structure, mesoscale structure and microscale structure information of coral reef pore structure, and form a fine identification and characterization method of “millimeter–micron–nanometer”-scale coral reef pore structure, which can improve data support for effectively solving the productivity prediction and evaluation of coral reef oil and gas reservoirs. It provides a new research perspective for the development of theoretical and technical models for the development characteristics of coral reef pore structure.

## 2. Multi-Scale Pore Image Acquisition Technology

According to the different characteristics of coral reef pore structure scale, the multi-scale pore structure of coral reef is divided into macroscale, mesoscale and microscale. The macroscale mainly reflects the millimeter-scale macropore structure of coral reefs.

The microscale mainly reflects the nanoscale micropore structure of coral reefs. The mesoscopic-scale between macroscale and microscale mainly reflects the micropore structure of coral reefs.

### 2.1. Macroscale Pore Structure Acquisition

The borehole camera technology commonly used in engineering logging is used to obtain the macroscale pore structure image of the coral reef. Borehole camera technology is to use the optical probe to go deep into the borehole of coral reef stratum and take continuous photos or videos of the borehole wall, so as to visually present the image information. The images analyzed in this paper are collected by the digital panoramic borehole camera system developed by the Institute of Rock and Soil Mechanics, Chinese Academy of Sciences [12–14]. The system is mainly composed of a panoramic probe, depth encoder, cable winch, control box and computer components. Its structural diagram is shown in Figure 1a. The maximum horizontal resolution of the equipment is 0.05 mm and the maximum vertical resolution is 0.1 mm.

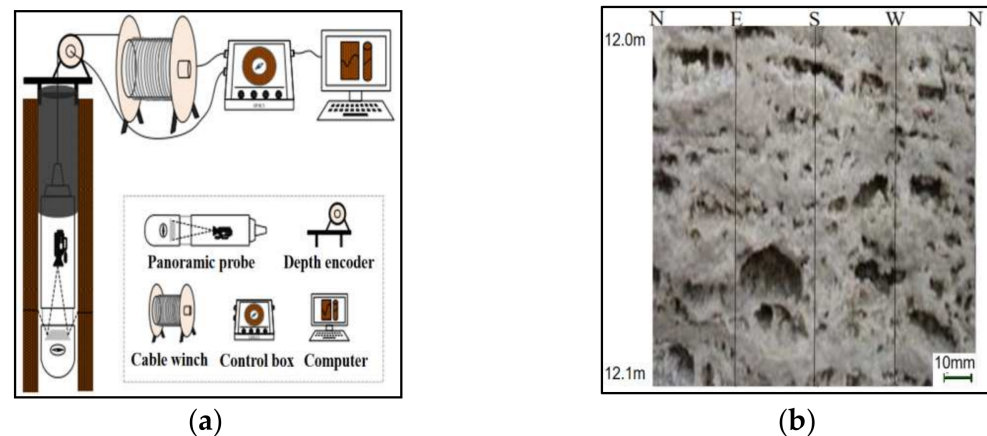


**Figure 1.** Structural diagram and plan expansion of borehole camera system. (a) Structural drawing of borehole camera system; (b) Plan expansion of borehole wall.

Taking the field geological borehole test data of a coral reef in the South China Sea as an example, the basic working principle of borehole camera technology is: 360° image data of the borehole wall is obtained by panoramic imaging technology, which usually includes an annular borehole wall image, depth information and azimuth information. Based on the digital image processing technology, the panoramic image is converted into a panoramic image, and the expanded plan of the coral reef borehole wall is shown in Figure 1b. Figure 1b is the expanded view of the borehole rock wall at the borehole depth of 12.0~12.1 m, and the actual size represented by the image is 100 mm × 100 mm. The left side of the borehole wall plan is due north, the horizontal length is the borehole perimeter and the vertical length is the borehole depth. The optical image of the pore wall can intuitively present the pore structure information of the coral reef. The coral reef skeleton is non-concave. Compared with the pore area, it has a better reflection effect on light, resulting in brighter optical features in the borehole image. Therefore, the borehole wall plan collected by the borehole camera technology can effectively present the macroscale pore structure characteristics of coral reefs.

### 2.2. Mesoscopic-Scale Pore Structure Acquisition

The mesoscale pore images of coral reefs are obtained by the combination of rock casting technology and an optical microscope. Rock pore cast thin section is a method to study the real pore size distribution in rock. It is mainly used to study the content, type and distribution of pores. It is convenient and economical to obtain, so it has more advantages. The biggest advantage of a rock pore cast thin section over a conventional thin section is

that the pore space is filled with dyed resin or liquid glue, which can easily and directly observe the pore space and avoid artificially induced pores and cracks.

Taking the actual core corresponding to the above borehole image as the test sample, the sample is reef limestone, with the size of 30 mm × 2 mm. The basic principle of rock pore casting thin slice is as follows: pay attention to the pore space of rock under vacuum, solidify the resin or liquid glue under a certain temperature and pressure, and then grind it into rock thin slice. Rock thin slice is a small rock slice cut upward from the vertical bedding direction of the rock specimen, adhered to the glass slide and ground into a 0.03 mm thick thin slice. Then, observe the size of the pores and throat and their interconnected and intersecting two-dimensional spatial structure under a polarizing microscope. The structure diagram of polarizing microscope technology is shown in Figure 2. Figure 2 is a polarizing micrograph of the drill core at the coral reef geological drilling depth of 12.0~12.1 m after processing the cast thin section. The actual size represented by the image is 200 μm × 200 μm. The difference between the rock casting thin slice and the ordinary thin slice is that the pores of the thin slice are filled with a special color organic resin (in this paper, the pores of the rock casting thin slice are filled with blue resin). These colored resin parts can represent the pore structure state of the two-dimensional space of the rock, and the pores of the rock casting thin slice can be easily detected through the color characteristics. Therefore, the combination of rock casting technology and optical microscopy to obtain coral reef pore casting thin sections can effectively present the mesoscopic pore structure characteristics of coral reefs.

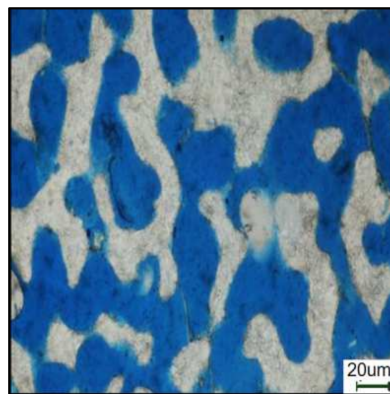


**Figure 2.** Cast thin section of coral reef.

### 2.3. Microscale Pore Structure Acquisition

The scanning electron microscope technology commonly used in the laboratory is used to obtain the microscale pore images of coral reefs. SEM is an electron microscope that uses an electron beam to scan the sample surface to obtain sample information. It mainly adopts the point-by-point imaging method to convert different features of the sample surface into video signals in order and proportion to form a frame image, so that various feature images of the sample surface can be observed on the fluorescent screen. Before the experiment, the shale sample needs to be pretreated manually and mechanically polished to a flat section. If the sample surface is damaged during the pretreatment, the observation of micropore structure will be blurred. After the pretreatment, Quanta400 environmental scanning electron microscope is used to test and analyze the micropore structure of the coral reef with an LED probe in low vacuum (106.7 Pa) mode.

Taking the actual core corresponding to the above borehole image as the test sample, the sample is reef limestone, with the size of 30 mm × 2 mm. The working principle of a scanning electron microscope is as follows: the electron beam (about 50 μm in diameter) is emitted from the electron gun and converged through the magnetic lens system under the action of accelerating voltage to form an electron beam with a diameter of 5 nm, which is focused on the sample surface. Under the action of the deflection coil between the second condenser and the objective lens, the electron beam performs grating scanning on the

sample, and the electron interacts with the sample to produce signal electrons. These signal electrons are collected by the detector and converted into photons, then amplified by the electrical signal amplifier, and finally imaged on the display system. The generated coral reef SEM image is shown in Figure 3. Figure 3 is the SEM image of the local area of the drilling core at the geological drilling depth of 12.0~12.1 m in the coral reef. The actual size represented by the image is  $200\text{ nm} \times 200\text{ nm}$ . In order to reduce the error, during the actual test, ten test areas are randomly selected on the surface of each sample, and then the ten test areas are tested, respectively, to obtain fifty SEM images. SEM images are gray-scale images, which can intuitively show the microstructure characteristics of nanoscale coral reefs. Therefore, SEM images collected by scanning electron microscope can effectively show the microscale pore structure characteristics of coral reefs.

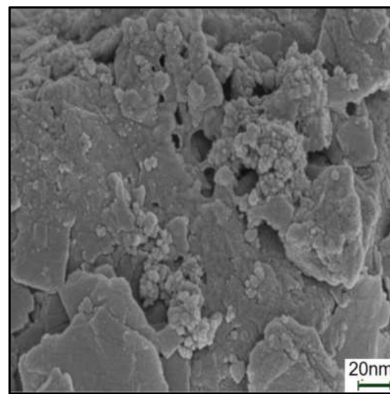


**Figure 3.** SEM image of coral reef.

### 3. Multi-Scale Pore Structure Identification Method

#### 3.1. Image Preprocessing

The main task of extracting multi-scale pore structure characteristic parameters of coral reefs is to effectively separate the pore structure from the background. However, the multi-scale pore structure image usually contains noise interference caused by multiple factors without processing. For example, in the process of logging, the illumination in the borehole is uneven, the camera conditions are bad and there is gradual interference caused by the test system in the acquisition process. These interferences greatly affect the image quality and can easily have a great impact on the subsequent feature recognition of the pore structure. Therefore, it is necessary to smooth the pore image of the coral reef to reduce the interference to the recognition as much as possible. In this paper, the multi-scale pore structure of the coral reef is preprocessed by the combination of image enhancement and filtering.

The effect of traditional image enhancement methods is not obvious, the peak signal-to-noise ratio is not high, the applicability is not strong and the global information is not well used to enhance the image details. In view of the unsatisfactory image enhancement effect, caused by a variety of degradation factors and which can be applied to multi-scale pore structure images from different information sources, an image enhancement method based on power-law transformation with a changing gamma value is proposed on the basis of the combination of global and local, that is, the improved gamma correction image enhancement method. Different images have different information and features. In the same image, the overall information is also closely related to the detailed information of the region. According to this information, we can better enhance the image. In order to determine the enhancement function more accurately, each pixel in the image needs to be classified. When the gray value of a pixel is greater than the average brightness, it is considered as a bright spot. When the gray value of a pixel is less than the average brightness, it is considered as a dark point. When the gray value of a pixel is equal to the average brightness, it is considered as a smooth point. Each pixel of the image is analyzed

and processed to determine the enhancement function more accurately. The average brightness of the extracted image is the characteristic component, and the expression of the average brightness  $v$  is:

$$v = \sum_{g=1}^L \frac{g}{L} \cdot \frac{i_g}{M \cdot N} \quad (1)$$

where  $L$  represents the image gray level and  $g$  represents the pixel gray value.  $i_g$  is the number of pixels of the image gray level  $g$ , and  $M$  and  $N$  are the total number of rows and columns of the image matrix, respectively. In order to reduce the enhancement amplitude of pixels with high brightness or darkness and increase the enhancement amplitude of relatively smooth pixels, this paper quantifies the enhancement amplitude of light and dark pixels unevenly, so that there is no ringing phenomenon in image enhancement. In this paper, the nonlinear transformation function is used to quantify the enhancement amplitude of pixels, and the expression of the enhancement function  $Z(g)$  is:

$$Z(g) = \frac{1}{1 + (v \cdot \frac{g}{L})^E} \quad (2)$$

where, the value range of  $Z(g)$  is  $(0, 1)$ , and  $E$  controls the slope of the function. When the gray value is closer to the average value  $v$ ,  $Z(g)$  is closer to 0.5, indicating that the pixel is relatively smooth and the contrast is relatively small; when the gray value is farther away from the average value  $v$  and  $Z(g)$  is closer to 0 or 1, it indicates that the darker or brighter the pixel, the greater the contrast. The traditional gamma correction has a certain gamma index value, which can only expand or compress a certain gray range. The algorithm in this paper first classifies each pixel in the image, quantifies the specific gray value to the range of  $(0, 1)$  through the nonlinear transformation function, and then adopts the changed gamma index value to enhance the image more accurately. The gray level with a low contrast is stretched to a wider range to enhance the contrast, and the gray level with a high contrast is stretched to a relatively narrow range. In gamma correction, the gamma index value controls the slope of the transformation function. The larger the gamma index, the steeper the transformation curve. The steeper the curve, the greater the gray value after transformation, and the greater the contrast. In this algorithm, the modified gamma index value is the difference between 1.5 and the enhancement function  $Z(g)$ . The improved gamma corrected image gray  $PF$  expression is:

$$PF_{out} = cPF_{in}^{(1.5-Z(g))} \quad (3)$$

where  $PF_{in}$  and  $PF_{out}$  are gray values of input and output images, respectively.  $c$  is a parameter that controls the shape of the conversion curve. The denoising effect of the median filter is ideal. It can filter out the noise points with obvious differences in pixel values, and effectively prevent the blurring of image details such as contour and edge. It is better than mean filter in suppressing salt and pepper noise and pulse interference, and can ensure the clarity of the edge. After the image enhancement processing is completed, the median filter algorithm is used to filter the image, so as to eliminate the noise points of numerical mutation. In order to avoid the interference of external information on image analysis, the image markers obtained by different technologies are removed in the multi-scale pore structure feature analysis of coral reefs in this paper. In this paper, MATLAB software is used for image analysis and processing, and a  $3 \times 3$  median filter is selected to process the multi-scale pore images in Figures 1b, 2b and 3b. The processed results are shown in Figure 4. From the comparison between Figure 4 and the original figure, it can be seen that using the modified gamma index value, the multi-scale pore structure images from different information sources can obtain satisfactory enhancement results.

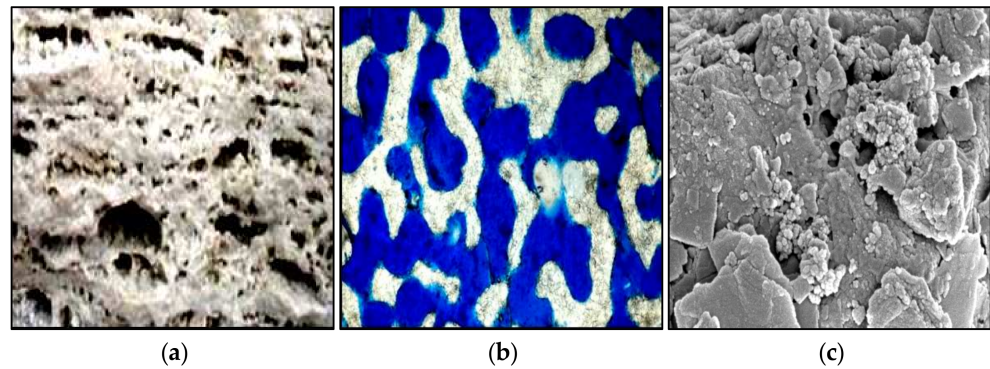


**Figure 4.** Multi-scale pore structure image after enhancement processing. (a) Macroscale image; (b) Mesoscale image; (c) Microscale image.

### 3.2. Pore Structure Identification

The key to coral reef multi-scale pore structure recognition is to find the best segmentation threshold of the image and binarize it. Finally, the binary image is processed by morphological operation to eliminate defects. Image segmentation refers to the technology and process of dividing the image into non overlapping regions with different characteristics according to the information of gray, color, texture and geometry, and extracting the target of interest, that is, to separate the target from the background in an image, so as to further analyze the target of interest. Figure 5 is the gray histogram of Figure 4. According to the characteristics of the histogram, an iterative image threshold segmentation algorithm is used to segment the original pore image to obtain the pores in the image. The iterative image threshold segmentation algorithm steps are as follows:

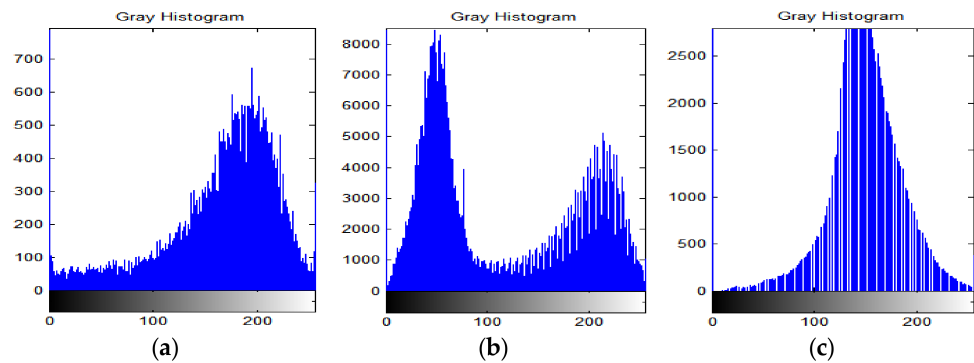


**Figure 5.** Gray histogram. (a) Macroscale image; (b) Mesoscale image; (c) Microscale image.

In step 1, the minimum gray value and the maximum gray value in the enhanced multi-scale pore structure image are calculated, and the initial threshold  $T_0$  is calculated;

$$T_0 = \frac{PF_{out}|_{\max} - PF_{out}|_{\min}}{2} \tag{4}$$

In step 2, the image is divided into the target and background according to the threshold, and the average gray value of the two parts is obtained.

$$\begin{cases} PF_{out}|_O = \frac{\sum PF_{out}(i,j) < T_K^{PF_{out}(i,j) \times N(i,j)}}{\sum PF_{out}(i,j) < T_K^{N(i,j)}} \\ PF_{out}|_G = \frac{\sum PF_{out}(i,j) > T_K^{PF_{out}(i,j) \times N(i,j)}}{\sum PF_{out}(i,j) > T_K^{N(i,j)}} \end{cases} \tag{5}$$

In the above formula,  $PF_{out}(i, j)$  is the gray value of point  $(i, j)$  on the image,  $N(i, j)$  is the weight coefficient of point  $PF_{out}(i, j)$ , generally  $N(i, j)$  is the number of points, and  $T_K$  is the threshold.

Step 3, re-select the threshold  $T_{k+1}$ .

$$T_{K+1} = \frac{PF_{out}|_O - PF_{out}|_G}{2} \quad (6)$$

Step 4, cycle from step 2 to step 4. When  $T_K = T_{K+1}$ , it ends, and the best threshold can be obtained for segmentation. After the threshold binarization segmentation of the image, the target boundary is often not smooth. At the same time, it is easy to spread some small noise interference on the background area. Before coral reef multi-scale pore structure recognition, it is also necessary to denoise the binary image of coral reef multi-scale pore structure. In this paper, mathematical morphology is used to smooth the object contour, in which the open operation is used to remove pepper noise and the closed operation is used to remove sandstone noise. If the open and close operations are used continuously, the front and background noise in the binary image can be significantly improved. After the image in Figure 5 is processed by this method, the image obtained is shown in Figure 6. The multi pore structure segmentation image of coral reef is defined by phase function. For the two-phase system considering only coral reef pores and the coral reef skeleton, when  $\vec{r}$  is located in coral reef pores, it is 1, and when  $\vec{r}$  is located in the coral reef skeleton phase, it is 0. The white areas represent pores in Figure 6.

$$P(\vec{r}) = \begin{cases} 1 & \vec{r} \in \text{coral reef pore} \\ 0 & \vec{r} \in \text{coral reef skeleton} \end{cases} \quad (7)$$

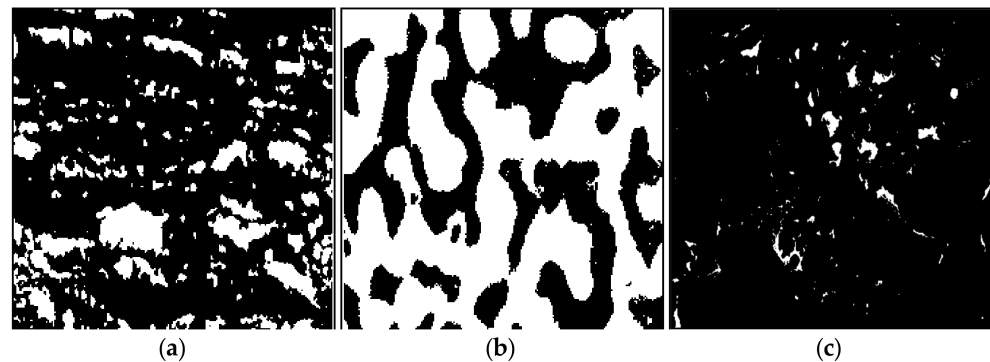


**Figure 6.** Image of coral reef after multi-scale pore structure recognition. (a) Macroscale image; (b) Mesoscale image; (c) Microscale image.

Combined with the analysis of the image characteristics of the coral reef pore structure at the “millimeter–micron–nanometer”-scale. The key area location search strategy of coral reef pore structure development characteristics is formulated, and the geometric feature extraction method is established. Combined with the energy difference characteristics of image pixels, a three-dimensional contour map of the optical enhancement map is established, as shown in Figure 7. From the figure, the pore or skeleton state of the coral reef pore structure can be clearly observed, which is convenient for the subsequent multi-scale pore structure characterization of coral reef. The legend value on the right in Figure 7 represents the corresponding gray value.

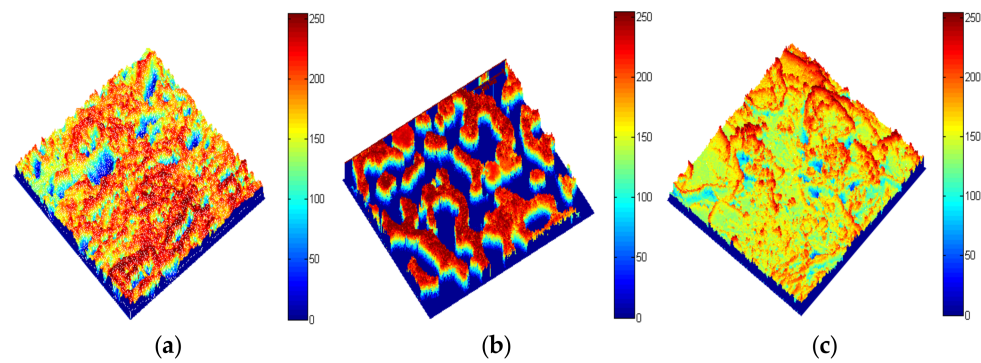


**Figure 7.** Three dimensional optical enhancement diagram of coral reef multi-scale pore structure. (a) Macroscale image; (b) Mesoscale image; (c) Microscale image.

#### 4. Multi-Scale Pore Structure Characterization Method

##### 4.1. Calculation of Characteristic Parameters

The single pore of the coral reef is a closed area composed of multiple white pixel sets connected with each other. Due to the different methods of obtaining the coral reef pore structure image, the parameter expression is also different in the calculation of the coral reef single pore structure characteristic parameters. In obtaining the radius of the coral reef pore area, the maximum circle search method is used for the radius search. If the number of pixels of the maximum inscribed circle radius of the coral reef pore area is  $N_r$  and the radius of the coral reef pore area is expressed in  $R$ , then the half diameter of the coral reef single pore structure is:

$$R = \begin{cases} \frac{2N_r \cdot \delta d}{\pi} & \text{Macro size} \\ N_r \cdot \delta d & \text{Non - macro size} \end{cases} \quad (8)$$

In the above formula,  $\delta d$  represents the actual size represented by each pixel. The longest axis of the boundary is defined as the Euclidean distance between the two farthest points on the outer boundary of the coral reef pore area. The farthest point on the boundary is not always unique, such as a point on a circle or square. Therefore, the following assumptions are made in the experiment: if the longest axis of the boundary is a useful descriptor, it is best to apply it to the boundary with a single farthest point pair. When there is more than one farthest point pair, they should be close to each other and are the main parameter to determine the shape of the boundary. The line segment connecting these points is called the longest axis of the boundary of the cell cavity. The minor axis of the boundary is defined as the line segment perpendicular to the longest axis of the boundary, which is recorded as  $D$ . The relationship between the longest axis and its short axis of the coral reef pore boundary is shown in Figure 8.

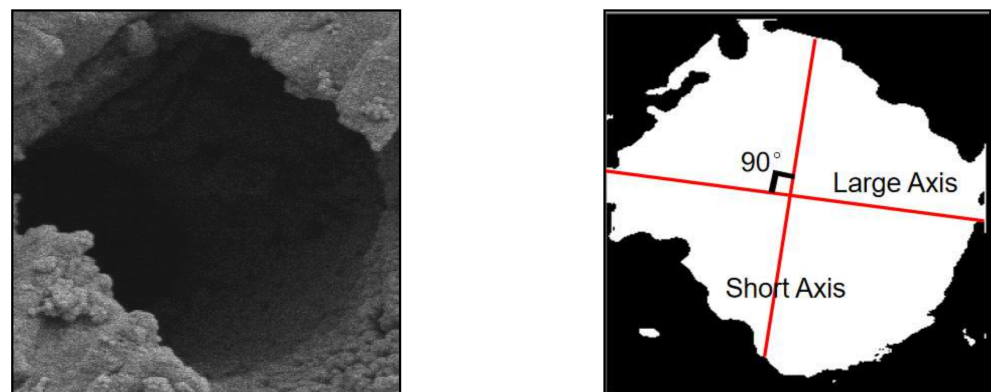


**Figure 8.** Relationship between the longest axis and its short axis of coral reef pore boundary.

The pore area represents the area formed by the set of pixels in the white closed area in the image, which is represented by  $S$ . The pore area is divided into an  $n \times n$  grid, the leftmost point of each row is  $P(x_i, y_{ij})$ , and the rightmost point is  $Q(x_i, y_{ij}')$ , then the pixel contained in it is  $y_{ij} - y_{ij}' + 1$ , and the area of the coral reef pore  $S$  is:

$$S = \begin{cases} \frac{1}{\pi} \cdot \delta d \cdot \delta d \cdot \sum_{i=1}^n (y_{ij} - y_{ij}' + 1) & \text{Macro size} \\ \frac{1}{2} \cdot \delta d \cdot \delta d \cdot \sum_{i=1}^n (y_{ij} - y_{ij}' + 1) & \text{Non - macro size} \end{cases} \tag{9}$$

The coral reef pore area represents the side length of the area composed of the outermost pixel set in the white closed area in the image, which is represented by  $C$ . The perimeter of the coral reef pore area is the length of chain code. By traversing the pore region contour point by point, the contour length obtained by statistical calculation is the perimeter of the pore region. Initialize perimeter  $C = 0$ , traverse all chain code elements of a single contour, if the chain code value is odd, then  $C = C + \sqrt{2}$ . If the chain code value is even, then  $C = C + 1$ . For each contour chain code, perform the above operations, and add all of the contour perimeter, that is, the total pore area perimeter  $C$ , the corresponding macro pore, and the corresponding pore area perimeter is  $2C/\pi$ . Because the shape of the coral reef pore area is very complex, in order to make the simplified pores have the same geometric characteristics as the real pores, it is necessary to evaluate the shape characteristics of the real coral reef pore area, that is, obtain the shape factor  $G$  of the coral reef pore area, which is defined as:

$$G = \frac{S}{C} \tag{10}$$

#### 4.2. Fractal Characterization

Fractal geometry takes a large number of non-smooth and irregular geometric shapes in nature and nonlinear systems as the research object, and aims to quantitatively describe complex shapes that are not suitable to be described by classical Euclidean geometry. Coral reef pores have a certain degree of self-similarity and fine structure, and have fractal characteristics. The shape of the pore section boundary can describe the regular characteristics of the pore. The pore perimeter of a certain area can reflect the pore geometry. The longer the peripheral curve length of the pore section, the greater the tortuosity of the pore boundary, the more irregular the pore geometry and the more complex the structure. Pore size distribution can characterize the homogeneous characteristics of the pore structure. The larger the range of pore size distribution, the more uneven the pore structure and the more obvious the heterogeneity of pores. In the calculation of a single scale fractal dimension, the island method is used to measure and calculate the fractal dimension of pore interface boundary [15]. The island method is a method to calculate the fractal dimension according to the measurement relationship. The existing relationship is:

$$\lg L(\varepsilon) = D_F \lg \alpha_D(\varepsilon) + \frac{D_F}{2} \lg A(\varepsilon) = C + \frac{D_F}{2} \lg A(\varepsilon) \tag{11}$$

where,  $C$  is the constant,  $L$  is the pore perimeter,  $A$  is the pore area,  $D_F$  is the fractal dimension,  $\varepsilon = \frac{l}{L_0}$ , where  $n$  is the absolute measurement scale and  $L_0$  is the perimeter of the initial figure. In the case of fixed scale  $n$ ,  $\alpha_D(\varepsilon)$  is a constant, and  $\alpha_D(\varepsilon)$  is only related to the selected scale, independent of the size of the graph. In the image, the perimeter and area of each pore are measured, respectively. The double logarithm plot of area and perimeter is twice the slope, which is the fractal dimension  $D_F$  value. According to the fractal description, the relationship between pore size distribution fractal and fractal dimension is as follows:

$$\lg N(r) = \lg a - D_F \lg r \tag{12}$$

where  $r$  is the equivalent radius of pores,  $N(r)$  is the number of pores with pore size greater than  $r$ , and  $a$  is a constant.

#### 4.3. Statistical Characterization

Auto correlation function  $S_x(r_1, r_2)$  is a parameter that can characterize the pore distribution characteristics of coral reefs. In order to reflect the multi-scale pore distribution of coral reefs, it is necessary to introduce an auto correlation function to characterize the statistical characteristics of the multi-scale pores of coral reefs. Auto correlation function is defined as the probability that any two points in the same scale image are distributed in the same pore. The auto correlation function represents the correlation between any two points in the same scale image. For the two-phase system, considering only coral reef pores and skeleton, its expression is:

$$S_x(r_1, r_2) = \overline{P(r_1) \times P(r_2)} \tag{13}$$

where  $r_1$  and  $r_2$  are any two points separated by a certain distance  $r$  in the same scale image.  $P$  is the value of the phase function. When the distance  $r = 0$ , the value of auto correlation function  $S_x(r_1, r_2)$  is the face gap of the image; When the distance  $r$  increases to a certain value, the auto correlation function tends to be stable. In order to reflect the change degree of regionalized variables in a certain direction and a certain distance, it is necessary to introduce a variation function  $\gamma(r)$ . The variation function of the same scale image is closely related to its structure. Variation function is an essential function to evaluate the properties of image structure. The expression of the variation function is:

$$\gamma(r) = \frac{1}{2N(r)} \sum_{i=1}^{N(r)} [P(r_i) - P(r_i + r)]^2 \tag{14}$$

where  $N(r)$  is the number of 2 points with distance  $r$  in the system.  $P(r_i)$  is the value at the  $r_i$  coordinate point.

### 5. Feature Region Location Method

On the basis of obtaining multi-scale coral reef pore structure images and characterization processing through multivariate testing technology, it is necessary to screen the key areas and refine the key location information to realize the location of multi-scale coral reef pore structure feature areas. In this section, according to the development characteristics of coral reef pore structure, the key area location search strategy of a multi-scale coral reef pore structure image is formulated to realize the key area location of the coral reef multi-scale pore structure.

#### 5.1. Search for Key Areas

In the search of key areas of coral reef multi-scale pore structure, the pore distribution characteristics, pore variation characteristics, pore fractal characteristics and pore shape characteristics in a certain range are combined, and the similarity matching algorithm is used to search the key areas of pores between different scales and different regions of the same scale. Let  $q$  be the target area image,  $t$  be the search area image,  $S_x$  represent the pore distribution feature similarity between the search area and the target area,  $\gamma$  represent the pore change feature similarity between the search area and the target area.  $D_F$  represents the pore shape feature similarity between the search area and the target area, and  $G_T$  represents the pore shape feature similarity between the search area and the target area. Then the comprehensive similarity  $DC$  between the two region images can be expressed as:

$$DC(q, t) = \frac{\lambda_a S_x + \lambda_b \gamma + \lambda_c D_F + \lambda_d G_T}{\lambda_a + \lambda_b + \lambda_c + \lambda_d} \tag{15}$$

where,  $\lambda_a$ ,  $\lambda_b$ ,  $\lambda_c$  and  $\lambda_d$  is the weighting of pore distribution characteristics, pore variation characteristics, pore fractal characteristics and pore shape characteristics, respectively. The commonly used image similarity matching algorithms mainly include the histogram intersection method, absolute distance method and Euclidean distance method. Although the Euclidean distance method has high retrieval accuracy, it has a large amount of calculation, resulting in a relatively slow operation speed. In order to obtain a high accuracy and abandon the advantage of speed, Euclidean distance is used in this paper. In the calculation of comprehensive similarity  $DC$ , the Euclidean distance  $L_{qt}$  from  $q$  to  $t$  is calculated, and the Euclidean distance  $L_{qt}$  represents the actual distance between the two regions. This distance combines the characteristics of pore distribution, pore variation, pore fractal and pore shape. The expression of Euclidean distance  $L_{qt}$  is:

$$L_{qt} = |q - t| = \sqrt{(q_1 - t_1)^2 + \dots + (q_M - t_M)^2} \leq M \quad (16)$$

In the key area search of pore structure at different scales, firstly, the parameters of pore distribution characteristics, pore variation characteristics, pore fractal characteristics and pore shape characteristics are artificially set, and the system automatically matches the target area image  $q$  on the specified scale image. Alternatively, by selecting the image of the designated area as the target area image  $q$ , the pore distribution characteristics, pore variation characteristics, pore fractal characteristics and pore shape characteristics are automatically calculated; then, the region image of the corresponding scale is selected from the images of different scales as the search region image  $t$ . Finally, according to the combination of pore distribution characteristics, pore change characteristics, pore fractal characteristics and pore shape characteristics in a certain range, and through the size of Euclidean distance  $L_{qt}$ , the distance ranking of pore key areas between different scales is realized. The nearest is the key area that needs to be searched and located.

## 5.2. Data Processing

The characteristic parameters of coral reef pore structure are calculated for the three images in Figure 6. After counting the continuous pixel area and ignoring the discrete single pixel, the number of pores corresponding to the macro-image is 198, the number of pores corresponding to the mesoscopic image is 47, and the number of pores corresponding to the micro-image is 226. The pore area radius  $r$ , pore area  $s$  and pore area perimeter  $C$  corresponding to the three characteristic images are shown in Figure 9. Figure 9a shows the distribution of pore characteristic parameters corresponding to macro-images. Figure 9b shows the distribution of pore characteristic parameters corresponding to mesoscopic images, and Figure 9c shows the distribution of pore characteristic parameters corresponding to micro-images.

As can be seen from Figure 9, the maximum radius of the macroscale pore structure is 8.6207 mm, the minimum radius is 0.2128 mm and the average radius is 1.1685 mm. The maximum area of the macroscale pore structure is 246.6274 mm<sup>2</sup>, the minimum area is 0.1811 mm<sup>2</sup> and the average area is 8.7411 mm<sup>2</sup>. The maximum perimeter of the macroscale pore structure is 79.1489 mm, the minimum perimeter is 1.7021 mm and the average perimeter is 10.5394 mm. The maximum radius of the mesoscopic pore structure is 14.4452 μm, the minimum radius is 0.4525 μm and the average radius is 1.0412 μm. The maximum area of the mesoscopic pore structure is 703.4929 μm<sup>2</sup>, the minimum area is 0.8190 μm<sup>2</sup> and the average area is 22.7394 μm<sup>2</sup>. The maximum perimeter of the mesoscopic pore structure is 123.0757 μm, the minimum perimeter is 3.6199 μm and the average perimeter is 8.6646 μm. The maximum radius of the microscale pore structure is 7.2876 nm, the minimum radius is 0.2558 nm and the average radius is 0.7794 nm. The maximum area of the microscale pore structure is 81.6321 nm<sup>2</sup>, the minimum area is 0.2616 nm<sup>2</sup> and the average area is 4.1527 nm<sup>2</sup>. The maximum perimeter of the microscale pore structure is 76.7263 nm, the minimum perimeter is 2.0460 nm and the average perimeter is 6.9936 nm. In the multi-scale pore structure characterization of coral reefs, the distribution diagrams corresponding to

the shape factor, fractal dimension, auto correlation function and variation function of coral reef pore area corresponding to the three characteristic images are shown in Figure 10, respectively. Among them, Figure 10a is the shape factor distribution diagram, Figure 10b is the fractal dimension distribution diagram, Figure 10c is the autocorrelation function distribution diagram, and Figure 10d is the variation function distribution diagram.

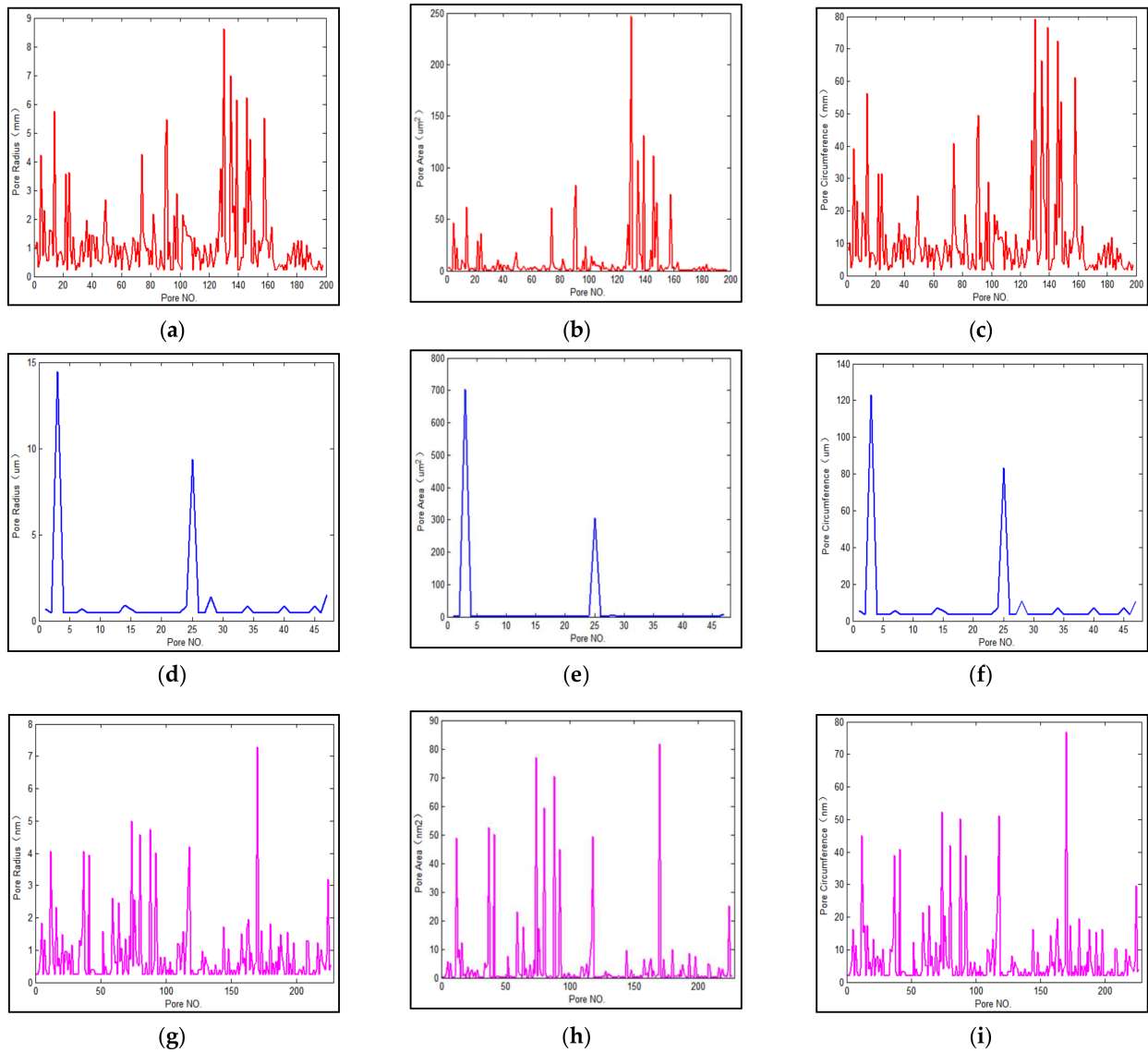


**Figure 9.** Distribution of multi-scale pore characteristic parameters. (a) Macropore radius; (b) Macropore area; (c) Macropore perimeter; (d) Mesoscopic pore radius; (e) Mesoscopic pore area; (f) Mesoscopic pore perimeter; (g) Micropore radius; (h) Micropore area; (i) Micropore perimeter.

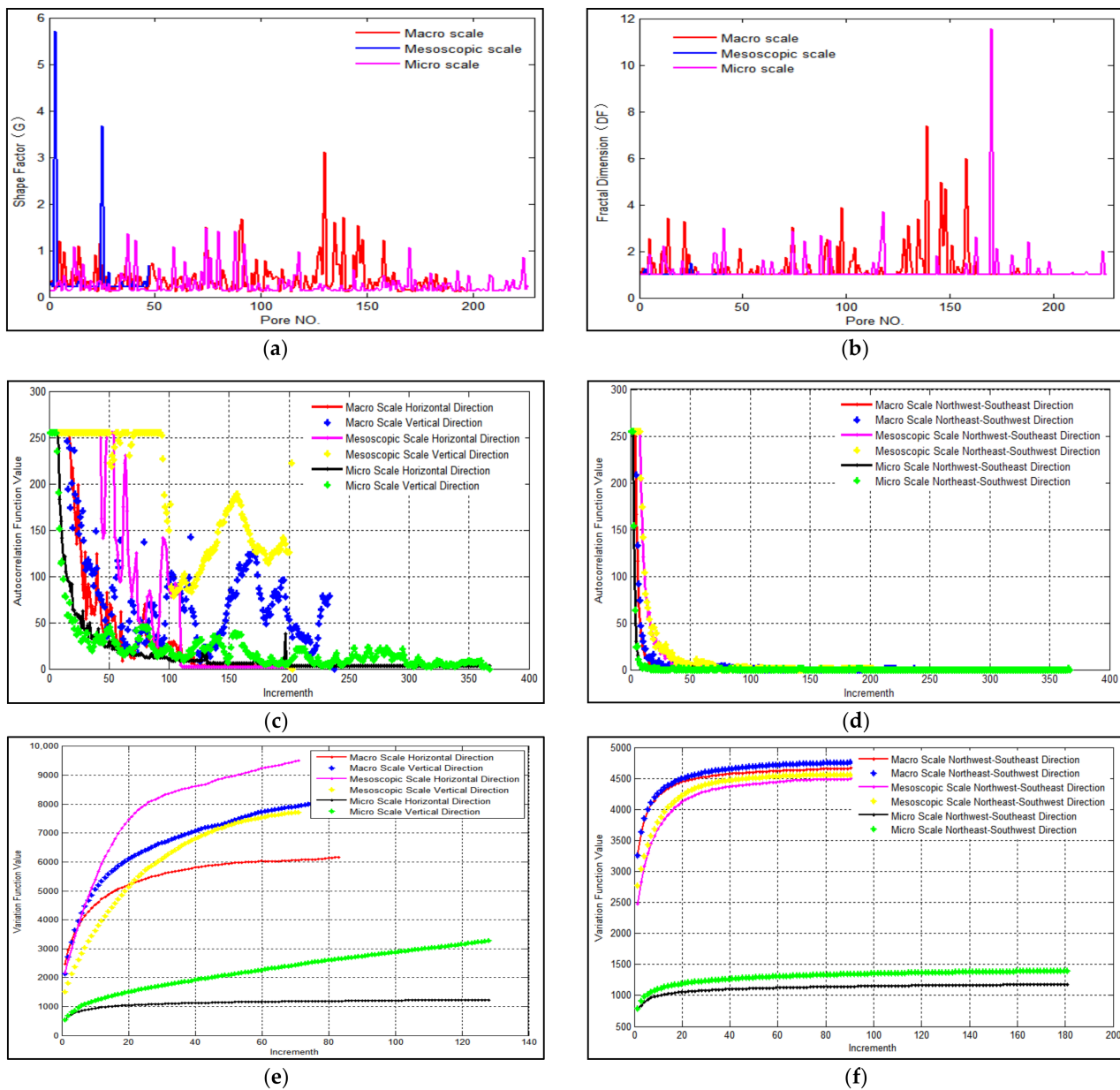


**Figure 10.** Numerical distribution of multi-scale pore structure characterization. (a) Shape factor; (b) Fractal dimension; (c) Horizontal and vertical autocorrelation functions; (d) Northwest–southeast and northeast–southwest autocorrelation functions; (e) Horizontal and vertical variation functions; (f) Northwest–southeast and northeast–southwest variation functions.

As can be seen from Figure 10, the maximum shape factor of the pore structure in macroscale is 3.1160, the minimum shape factor is 0.1064 and the average shape factor is 0.3839. The maximum fractal dimension is 7.3960, the minimum fractal dimension is 1 and the average fractal dimension is 1.3126. The average auto correlation function of the macroscale pore structure in the horizontal direction is 41.6008. The average auto correlation function of macroscale pore structure in the vertical direction is 84.4118. The average auto correlation function of the mesoscopic pore structure in the northwest–southeast direction is 7.4580. The average auto correlation function value of the macroscale pore structure in the northeast–southwest direction is 8.4202. The average variation function of the macroscale pore structure in the horizontal direction is 0.0055. The average variation function value of the macroscale pore structure in the vertical direction is 0.0068. The average variogram value of the macroscale pore structure in the northwest–southeast direction is 0.0045. The

average variogram value of the macroscale pore structure in the northeast–southwest direction is 0.0046.

The maximum shape factor of the mesoscopic pore structure is 5.7159, the minimum shape factor is 0.2262 and the average shape factor is 0.4494. The maximum fractal dimension of the mesoscopic pore structure is 1.4855, the minimum fractal dimension is 1 and the average fractal dimension is 1.0153. The average auto correlation function of the mesoscopic pore structure in the horizontal direction is 92.4089. The average auto correlation function of the mesoscopic pore structure in the vertical direction is 187.0043. The average auto correlation function of the mesoscopic pore structure in the northwest–southeast direction is 17.3793. The average auto correlation function of the mesoscopic pore structure in the northeast–southwest direction is 18.7192. The average variation function of the mesoscopic pore structure in the horizontal direction is 0.0078. The average variation function of the mesoscopic pore structure in the vertical direction is 0.0060. The average variogram value of the mesoscopic pore structure in the northwest–southeast direction is 0.0042. The average variogram value of the mesoscopic pore structure in the northeast–southwest direction is 0.0043.

The maximum shape factor of the microscale pore structure is 1.4743, the minimum shape factor is 0.1279 and the average shape factor is 0.2658. The maximum fractal dimension of the microscale pore structure is 11.5448, the minimum fractal dimension is 1 and the average fractal dimension is 1.1821. The average auto correlation function of the microscale pore structure in the horizontal direction is 18.0627. The average auto correlation function of the microscale pore structure in the vertical direction is 24.8910. The average auto correlation function of the microscale pore structure in the northwest–southeast direction is 2.2561. The average auto correlation function value of the microscale pore structure in the northeast–southwest direction is 2.3297. The average variation function of the microscale pore structure in the horizontal direction is 0.0011. The average variation function of the microscale pore structure in the vertical direction is 0.0023. The average variogram value of the microscale pore structure in the northwest–southeast direction is 0.0011. The average variogram value of the microscale pore structure in a northeast–southwest direction is 0.0013.

### 5.3. Result Analysis

It can be seen from the calculation results in the previous section that there are differences in the pore structure parameters and characterization characteristics at different scales. In order to more intuitively display the different characteristics of the pore structure between different scales, by comparing and analyzing the parameters between different scales, the distribution diagram of multi-scale pore structure characteristic parameters is shown in Figure 11. As can be seen from Figure 11a,d, the radii of pores with different scales are mainly distributed in 0–1 mm, 0–1  $\mu\text{m}$  and 0–1 nm, and the cumulative proportion reaches 72%. The radii of pores with different scales are less distributed in areas  $> 2$  mm,  $> 2$   $\mu\text{m}$  and  $> 2$  nm, respectively, and their cumulative proportion is about 9%. It can be seen from Figure 11b,e that the areas of pores with different scales are mainly distributed in 0–1  $\text{mm}^2$ , 0–1  $\mu\text{m}^2$  and 0–1  $\text{nm}^2$ , and the cumulative proportion reaches 52%. The pore areas of different scales are less distributed in the areas of 1–2 mm, 1–2  $\mu\text{m}$  and 1–2 nm, respectively, and the cumulative proportion is about 14%. It can be seen from Figure 11c,d that the perimeter of pores with different scales are mainly distributed in 0–5 mm, 0–5  $\mu\text{m}$  and 0–5 nm, and the cumulative proportion reaches 53%. The perimeter of pores with different scales is evenly distributed in other areas, accounting for 24% in the areas of 5–10 mm, 5–10  $\mu\text{m}$  and 5–10 nm, and 23% in the areas of  $>10$  mm,  $>10$   $\mu\text{m}$  and  $>10$  nm.

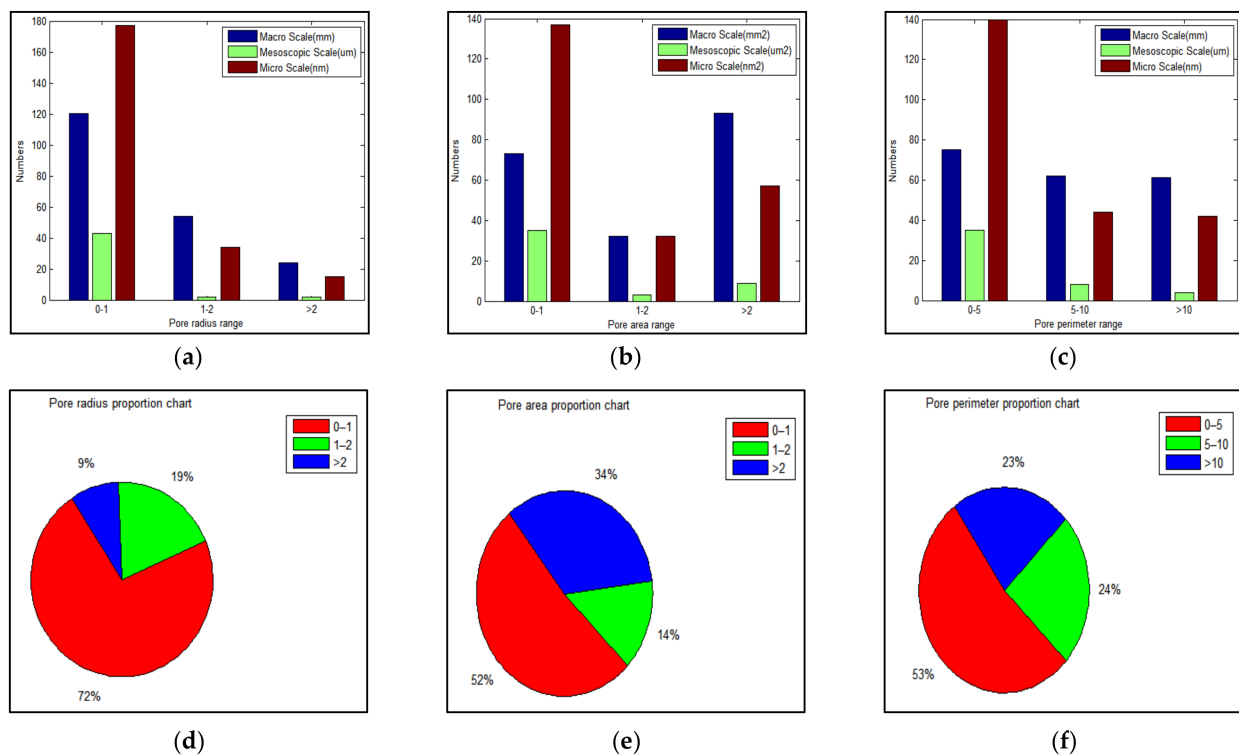
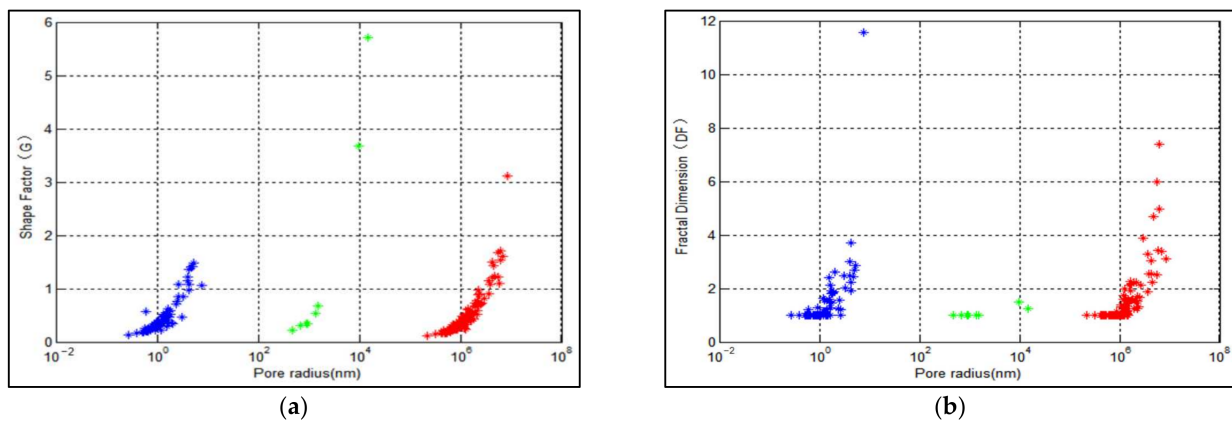


**Figure 11.** Distribution of characteristic parameters of multi-scale pore structure. (a) Radius quantity distribution histogram; (b) Area quantity distribution histogram; (c) Perimeter quantity distribution histogram; (d) Radius quantity distribution proportion diagram; (e) Area quantity distribution proportion diagram; (f) Perimeter quantity distribution proportion diagram.

The blue dots in Figure 12 represent macropores, the green dots represent mesoscopic pores, and the red dots represent micropores. The relationship between pore radius and shape factor is shown in Figure 12a. It can be seen from the Figure 12a that the macro-image shape factor obtained by drilling camera technology is mainly distributed at about 0.38, the mesoscopic image shape factor obtained by rock casting sheet technology is mainly distributed at about 0.45, and the micro-image shape factor obtained by scanning electron microscope technology is mainly distributed at about 0.27. The relationship between pore radius and fractal dimension is shown in Figure 12b. It can be seen from the Figure 12 that the fractal dimension of the macro-image obtained by drilling camera technology is mainly distributed around 1.31, the fractal dimension of the mesoscopic image obtained by rock casting thin section technology is mainly distributed around 1.49, and the fractal dimension of the micro-image obtained by scanning electron microscope technology is mainly distributed around 1.18. This shows that the characteristic information of the pore structure images with different scales can be comprehensively reflected by using borehole camera technology, rock casting thin section technology and scanning electron microscope technology.

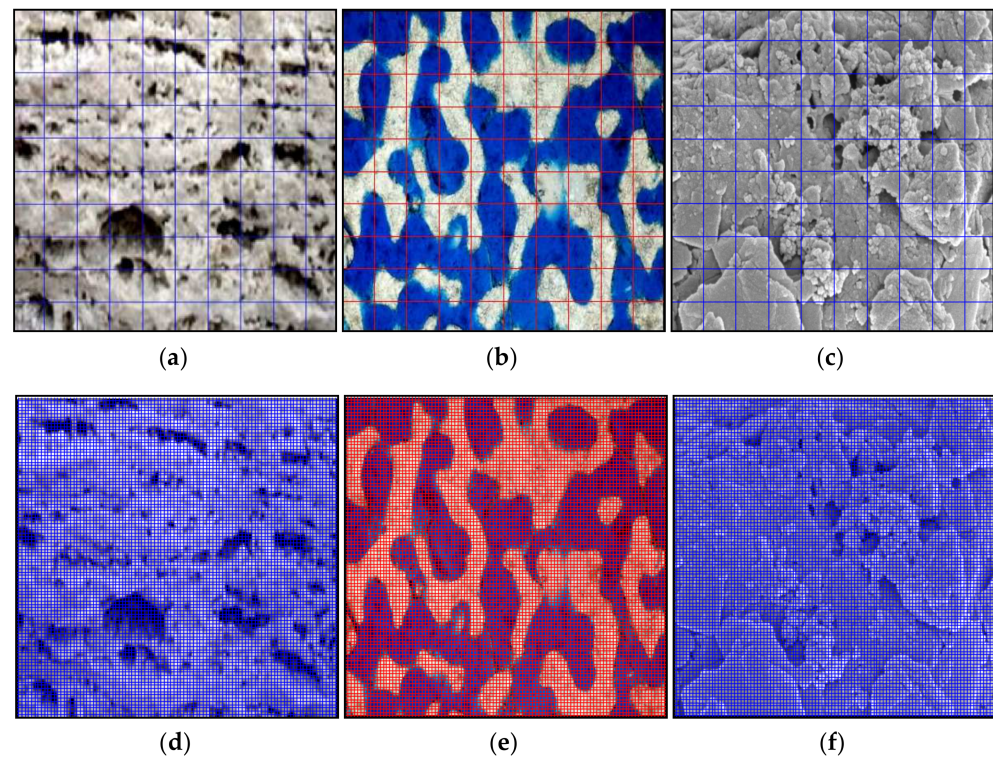
Based on the multi-scale coral reef pore structure image obtained by multivariate testing technology and characterization processing, the multi-scale coral reef pore structure characteristic area is located. The multi-scale coral reef pore structure image is the three in a sequence. In the search of key areas of coral reef multi-scale pore structure, the pore distribution characteristics, pore variation characteristics, pore fractal characteristics and pore shape characteristics in a certain range are combined, and the similarity matching algorithm is used to search the key areas of pores between different scales and different regions of the same scale. According to the relationship in Equation (10), the pairwise comprehensive similarity DC of the three images in Figure 4 is calculated. When  $t$  is the whole image area, the comprehensive similarity DC value between the macro-image in

Figure 4a and the mesoscopic image in Figure 4b is 0.6081. The comprehensive similarity DC value between the macro-image in Figure 4a and the micro-image in Figure 4c is 0.5840. The comprehensive similarity DC value between the mesoscopic image in Figure 4b and the microscopic image in Figure 4c is 0.3873. According to Equation (11), it can be calculated that the Euclidean distance between the macro-image in Figure 4a and the mesoscopic image in Figure 4b is 0.3919, and the Euclidean distance between the macro-image in Figure 4a and the micro-image in Figure 4c is 0.4160. The Euclidean distance between the mesoscopic image in Figure 4b and the microscopic image in Figure 4c is 0.6127. That is, the Euclidean distance between the mesoscopic image in Figure 4b and the micro-image in Figure 4c is the largest, and the Euclidean distance between the macro-image in Figure 4a and the mesoscopic image in Figure 4b is the smallest. It is explained that the similarity between the macro-image in Figure 4a and the mesoscopic image in Figure 4b is the highest, which is mainly due to the smaller difference between the mesoscopic-scale image and the macroscale image, and the larger difference between the mesoscopic-scale image and the microstructure features, which verifies the correctness of the characterization method described in this paper.



**Figure 12.** Distribution of multi-scale pore structure characterization parameters. (a) Pore radius and shape factor; (b) Pore radius and fractal dimension.

Although the Euclidean distance between the macro-image in Figure 4a and the micro-image in Figure 4c is the smallest, there is still a large gap, which is mainly due to the order of magnitude difference in the scales represented by the three images. The mesoscopic image in Figure 4b is a small part of the macro-image in Figure 4a, while the micro-image in Figure 4c is a small part of the mesoscopic image in Figure 4b. Therefore, in order to verify the correctness and accuracy of the method in this paper, the three images in Figure 4 are meshed by  $10 \times 10$  and  $100 \times 100$  respectively, as shown in Figure 13. Then, the comprehensive similarity and Euclidean distance of the meshed images are calculated respectively.



**Figure 13.** Grid division of multi-scale pore structure image. (a)  $10 \times 10$  macro-image; (b)  $10 \times 10$  mesoscopic image; (c)  $10 \times 100$  micro-image; (d)  $100 \times 100$  macro-image; (e)  $100 \times 100$  mesoscopic image; (f)  $100 \times 100$  micro-image.

In the key area search of  $10 \times 10$  grid image, the search of the corresponding area in the macro-image is determined according to the mesoscopic image. Firstly, the mesoscopic image is selected as the target region, and then the region image matrix  $[1, 1]$  in the macro-image is used as the search region, and the comprehensive similarity of the two region images is calculated. After the search of the area image matrix  $[1, 1]$  in the macro-image is completed according to the search method in Section 5.1, the area image matrix  $[1, 2]$  in the macro-image is taken as the search area, and so on until the search of the area image matrix  $[10, 10]$  in the macro-image is completed, and the search results are shown in Figure 14a. In the key area search of  $10 \times 10$  grid image, the search of the corresponding area in the mesoscopic image is determined according to the micro-image. Firstly, the micro-image is selected as the target region, and then the region image matrix  $[1, 1]$  in the mesoscopic image is used as the search region, and the comprehensive similarity of the two region images is calculated. After completing the search of the area image matrix  $[1, 1]$  in the mesoscopic image, take the area image matrix  $[1, 2]$  in the mesoscopic image as the search area, and so on until the search of the area image matrix  $[10, 10]$  in the mesoscopic image is completed. The search results are shown in Figure 14b. In the key area search of  $10 \times 10$  grid image, the search of the corresponding area in the macro-image is determined according to the micro-image. Firstly, the micro-image is selected as the target area, and then the regional image matrix  $[1, 1]$  in the macro-image is used as the search area, and the comprehensive similarity of the two regional images is calculated. After completing the search of the area image matrix  $[1, 1]$  in the macro-image, take the area image matrix  $[1, 2]$  in the macro-image as the search area, and so on until the search of the area image matrix  $[10, 10]$  in the macro-image is completed, and the search results are shown in Figure 14c.

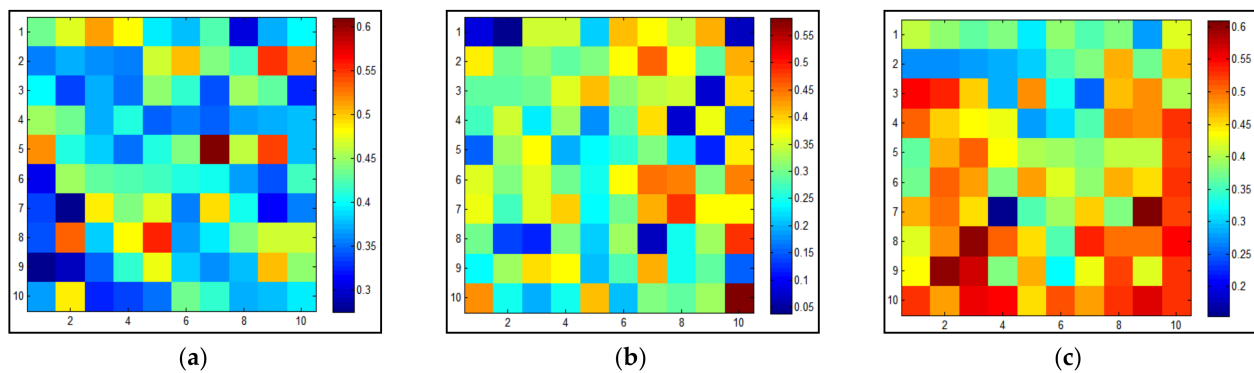


**Figure 14.**  $10 \times 10$  grid multi-scale pore structure image search diagram. (a) Macro mesoscopic search; (b) Mesoscopic micro search; (c) Macro micro search.

As can be seen from Figure 14a, the maximum comprehensive similarity value is 0.6104, and the corresponding search matrix is row 5 and column 7, indicating that the comprehensive similarity between the regional image matrix [5, 7] in the macro-image and the mesoscopic image is the highest. As can be seen from Figure 14b, the maximum comprehensive similarity value is 0.5824, and the corresponding search matrix is row 10 and column 10, indicating that the regional image matrix [10, 10] in the mesoscopic image has the highest comprehensive similarity with that in the microscopic image. As can be seen from Figure 14c, the maximum comprehensive similarity value is 0.6099, and the corresponding search matrix is row 7 and column 9, indicating that the comprehensive similarity between the regional image matrix [7, 9] in the macro-image and the micro-image is the highest.

In the key area search of  $100 \times 100$  grid image, the search of the corresponding area in the macro-image is determined according to the mesoscopic image. Firstly, the mesoscopic image is selected as the target region, and then the region image matrix [1, 1] in the macro-image is used as the search region, and the comprehensive similarity of the two region images is calculated. After completing the search of the area image matrix [1, 1] in the macro-image, take the area image matrix [1, 2] in the macro-image as the search area, and so on until the search of the area image matrix [100, 100] in the macro-image is completed, and the search results are shown in Figure 15a. In the key area search of  $100 \times 100$  grid image, the search of the corresponding area in the mesoscopic image is determined according to the micro-image. Firstly, the micro-image is selected as the target region, and then the region image matrix [1, 1] in the mesoscopic image is used as the search region, and the comprehensive similarity of the two region images is calculated. After completing the search of the area image matrix [1, 1] in the mesoscopic image, take the area image matrix [1, 2] in the mesoscopic image as the search area, and so on until the search of the area image matrix [100, 100] in the mesoscopic image is completed, and the search results are shown in Figure 15b. In the key area search of  $100 \times 100$  grid image, the search of the corresponding area in the macro-image is determined according to the micro-image. Firstly, the micro-image is selected as the target area, and then the regional image matrix [1, 1] in the macro-image is used as the search area, and the comprehensive similarity of the two regional images is calculated. After completing the search of the area image matrix [1, 1] in the macro-image, take the area image matrix [1, 2] in the macro-image as the search area, and so on until the search of the area image matrix [100, 100] in the macro-image is completed, and the search results are shown in Figure 15c. The value in the legend on the right in Figure 15 represents the similarity value. The larger the value, the higher the pixel.

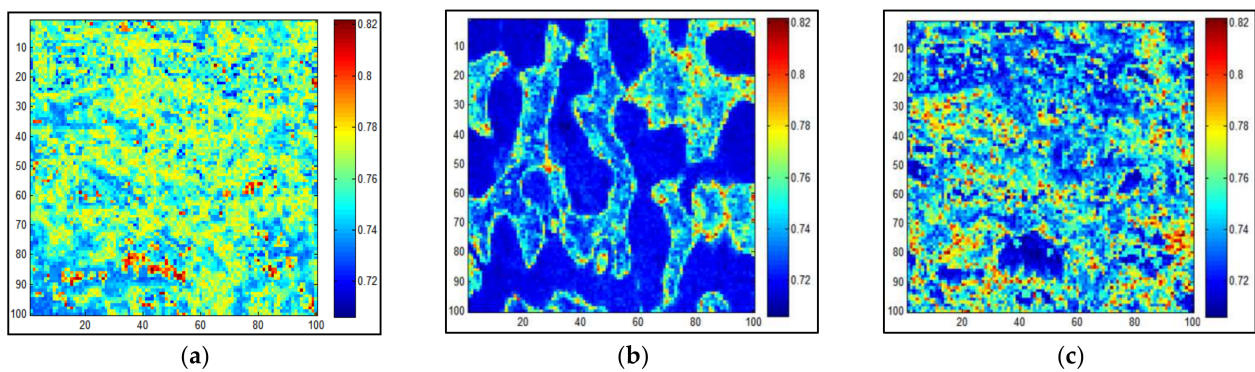


**Figure 15.**  $100 \times 100$  grid multi-scale pore structure image search diagram. (a) Macro mesoscopic search; (b) Mesoscopic micro search; (c) Macro micro search.

As can be seen from Figure 15a, the maximum value of comprehensive similarity is 0.8220, and the corresponding search matrix is row 81 and column 35, indicating that the comprehensive similarity between the regional image matrix [81, 35] in the macro-image and the mesoscopic image is the highest. As can be seen from Figure 15b, the maximum comprehensive similarity value is 0.8216, and the corresponding search matrix is row 17 and column 77, indicating that the comprehensive similarity between the regional image matrix [17, 77] in the mesoscopic image and the micro-image is the highest. As can be seen from Figure 15c, the maximum value of comprehensive similarity is 0.7644, and the corresponding search matrix is row 85 and column 49, indicating that the comprehensive similarity between the regional image matrix [85, 49] in the macro-image and the micro-image is the highest. In order to verify the accuracy of the method in this paper, the key area search results of  $10 \times 10$  grid image, the key area search results of  $100 \times 100$  grid image and the area where the real extracted image is located are compared. The comparison diagram between the search positioning area and the real sampling area is shown in Figure 16. Figure 16a searches for the sampling area corresponding to the macroscale through the mesoscopic image. Figure 16b is a microscopic image for searching the sampling area corresponding to the mesoscopic-scale. Figure 16c is a diagram for searching the sampling area corresponding to the macroscale through the micro-image. The dark red area in the Figure represents the real sampling area, the pink area represents the  $10 \times 10$  grid search positioning area, and the green area represents the  $100 \times 100$  grid search positioning area.

As can be seen from Figure 16a, in searching the sampling area corresponding to the macroscale through the mesoscopic image, the  $100 \times 100$  grid is used for search, and the calculated positioning area is closer to the real sampling area. As can be seen from Figure 16b, in searching the sampling area corresponding to the mesoscopic-scale through the micro-image, a  $100 \times 100$  grid is used for search, and the calculated positioning area is closer to the real sampling area. As can be seen from Figure 16c, in searching the sampling area corresponding to the macroscale through the micro-image, the  $100 \times 100$  grid is used for the search, and the calculated positioning area is closer to the real sampling area. This is mainly because the real sampling size area is small, and the  $100 \times 100$  grid division is carried out more than the  $10 \times 10$  grid division, and the divided search area is closer to the real area. In taking the macroscale image as the search target image, the reliability of taking the mesoscopic-scale image as the target area is higher than that of taking the micro-scale image as the target area, mainly because the mesoscopic-scale is closer to the macro-scale pore structure characteristics than the microscale. Through this comparison, the feasibility and correctness of this method are also verified.

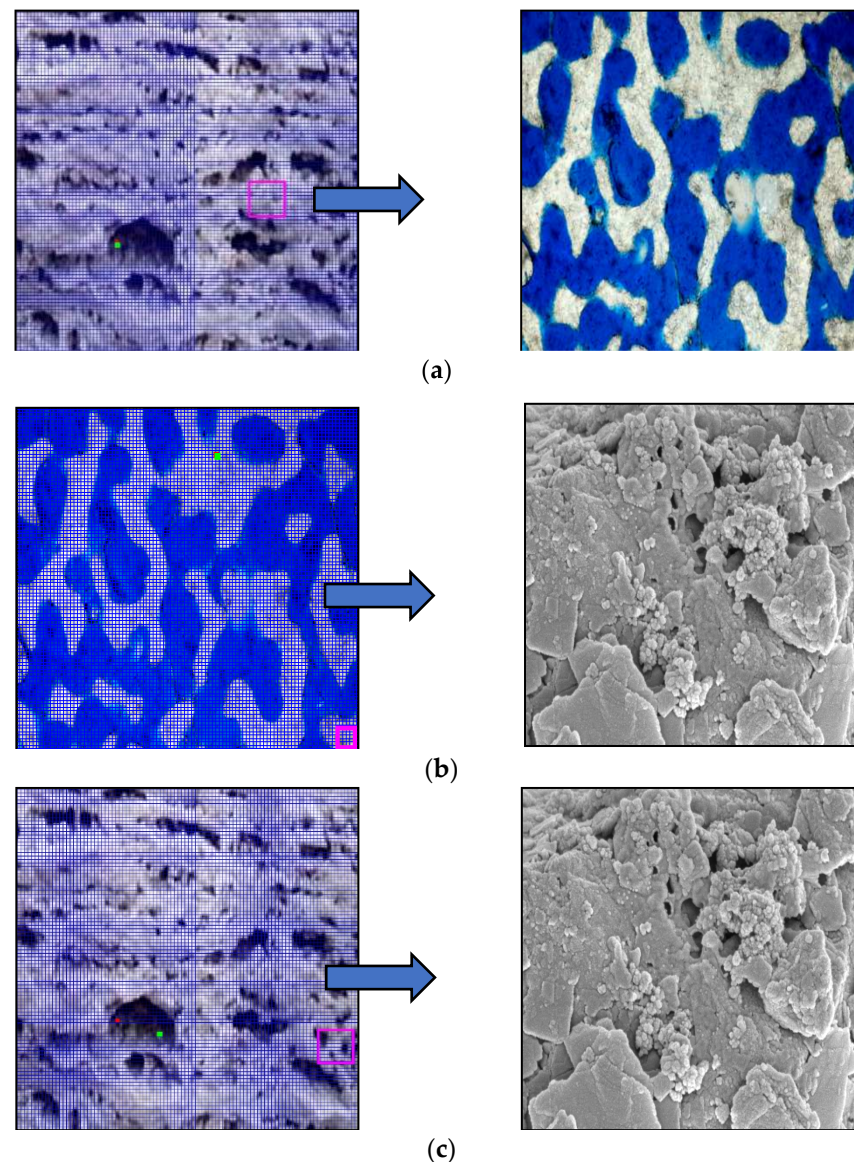


**Figure 16.** Comparison between search location area and real sampling area. (a) Macro mesoscopic search positioning comparison; (b) Meso-micro search positioning comparison; (c) Macro micro search positioning comparison.

In addition, because the grid search method in this paper combines pore distribution characteristics, pore change characteristics, pore fractal characteristics and pore shape characteristics, in order to verify the advantages of this method, this method is compared with the grid search method considering only single pore characteristics, and  $100 \times 100$  grid search is realized through a similarity matching algorithm. The search location area corresponding to different methods is shown in Figure 17. Figure 17a is a search for the sampling area corresponding to the macroscale through the mesoscopic image. Figure 17b is a microscopic image to search the sampling area corresponding to the mesoscopic-scale. Figure 17c is a microscopic image to search the sampling area corresponding to the macroscale. The dark red area represents the real sampling area. The green area represents the  $100 \times 100$  grid search and location area processed by this method. The white area represents the  $100 \times 100$  grid search and location area considering only the pore distribution characteristics. The black area represents the  $100 \times 100$  grid search and location area considering only the pore change characteristics. The yellow area represents the  $100 \times 100$  grid search and location area considering only the pore fractal characteristics.

The pink area represents the location area of  $100 \times 100$  grid search considering only the shape characteristics of pores.

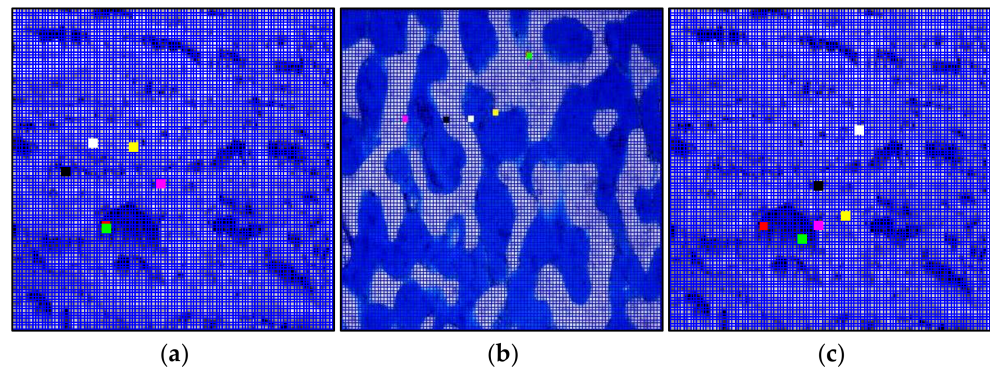


**Figure 17.** Comparison of search and location area results by different methods. (a) Macro-mesoscopic search; (b) Mesoscopic-micro search; (c) Macro-micro search.

As can be seen from Figure 17, the green area is closer to the dark red area than other color areas, which shows that the results obtained by the sampling method in this paper are closer to the real situation than the search method considering only the characteristics of a single factor. This is mainly because different pore structures show different characteristics in pore distribution characteristics, pore variation characteristics, pore fractal characteristics and pore shape characteristics. After combining a variety of pore characteristics, the similarity is higher and the corresponding search results will be more accurate. Therefore, through this comparison, the superiority of this method is also verified.

The multi-scale pore structure identification and characterization method of coral reef can obtain more comprehensive results in the process of the pore structure feature area search, because the correct multi-scale pore structure identification, parameter calculation and structure characterization methods are adopted. The experience of porosity determination by traditional manual methods is valuable, but the objective factors such as test environment and facilities and human subjective factors will inevitably introduce man-made random errors. Due to the local color difference of the collected images caused by uneven or light reflection, color segmentation of such images will produce a lot of holes, and the bonding between pores will also form a number of holes. Too many pores will seriously affect the segmentation quality of the image and cause inaccurate pore calculation. There will be errors between the porosity obtained by image analysis and the value measured by a manual method. The multi-scale coral reef pore structure recognition method described in this paper combines the image difference characteristics of coral reef pore structure at the “millimeter-micron-nanometer”-scale to establish a geometric feature extraction method for the development characteristics of coral reef pore structure. Combined with the energy difference characteristics of image pixels, the contour three-dimensional map of optical enhancement map can be established, and the pore or skeleton state of coral reef pore structure can be clearly observed from the map.

Through the calculation in this paper, the pore recognition structure of the image processing method is relatively stable, and the possibility of error at any time is small. The error is less than 0.5%. Based on the key area location search strategy combined with the development characteristics of the coral reef pore structure, it can effectively search the basic data sources of different scale images, and the results are coincident with the actual situation, which verifies the feasibility and correctness of this method. If the number of test samples and grid segmentation density can be increased, the accuracy of calculation and search will be higher. The main advantage of the method described in this paper is that it can realize the automatic identification and quantitative characterization of the coral reef pore structures at different scales, effectively solve the organic integration of the field engineering test and indoor precision test, provide a more accurate search strategy for a

special area search of pore structures at different scales, and search and inversely calculate the data source of the image according to the target image, It can provide good technical support for special area classification and a characteristic area search of pore structure. The method described in this paper also has some limitations. Because the data sources of the method described in this paper are all from the intuitive images of pore structure, if the image acquisition quality is poor, it will affect the accuracy of the whole method. Therefore, in the follow-up research, we need to further improve and perfect the calculation method, and add other technical means and methods to make up for the shortcomings of this technology and weaken the influence of image quality on the characterization results.

## 6. Conclusions

By using multivariate information acquisition technology, this paper constructs the multi-scale structure information correlation and fusion function of coral reef pore structure, and forms a fine identification and characterization method of “millimeter–micron–nanometer”-scale coral reef pore structure. The results show that: (1) this method can be applied to the identification and characterization of coral reef pore structure with different scales, different information sources and different degrees of precision. (2) This method can realize the correlation and data fusion of macro-structure, meso-structure and micro-structure information of the coral reef pore structure. (3) The pore structure of coral reefs at different scales has a certain correlation, which can be quantitatively characterized in combination with the characteristics of different dimensions of pore structure. (4) There are some differences in the test results obtained by different test methods, which can be normalized from the perspective of the image.

**Author Contributions:** Conceptualization, J.W.; Data curation, Q.G. and W.C.; Investigation, H.L. All authors have read and agreed to the published version of the manuscript.

**Funding:** This research was funded by the National Natural Science Foundation for the Youth of China (41902294); the Opening Foundation of Guangxi Laboratory on the Study of Coral Reefs in the South China Sea (GXLSRSCS2020003); the Opening Foundation of Key Laboratory of Carbonate Reservoir of CNPC (RIPED-2020-JS-51018).

**Institutional Review Board Statement:** Not applicable.

**Informed Consent Statement:** Not applicable.

**Data Availability Statement:** All data, models, and code generated or used during the study appear in the submitted article.

**Acknowledgments:** All the images and data are from our actual tests and permitted by the owners. We are compliant with ethical standards, and all authors declare that this paper has no conflict of interest. Finally, we are grateful for the many helpful and constructive comments from many anonymous reviewers.

**Conflicts of Interest:** The authors declare no conflict of interest.

## References

1. Chen, S.; Ren, D.C.; Li, J.M.; Xia, T.; Wang, D.; Du, G.Y.; Wang, Q.X.; Ke, S.Y.; Wang, L.; Wang, M.; et al. Concept and attribute definition of marine ecological capital. *J. Ecol.* **2010**, *30*, 6323–6330.
2. Wang, J.C.; Wang, C.Y. The integrity evaluation method of coral reef rock mass. *Geotech. Mech.* **2014**, *35*, 2934–2940.
3. Reaka-Kudla, M.L. The global biodiversity of coral reefs: A comparison with rainforests. In *Biodiversity II: Understanding and Protecting Our Natural Resources*; Reaka-Kudla, M.L., Wilson, D.E., Wilson, E.O., Eds.; National Academy Press: Washington, DC, USA, 1997; pp. 83–108.
4. David, W.S.; Olof, L. The health and future of coral reef systems. *Ocean. Coast. Manag.* **2000**, *43*, 657–688. [[CrossRef](#)]
5. Margheritini, L.; Moldrup, P.; Simonsen, M.E. Innovative Material Can Mimic Coral and Boulder Reefs Properties. *Front. Mar. Sci.* **2021**, *1*, 750. [[CrossRef](#)]
6. Han, D.N.; My, N.; Michihiro, I. A metabarcoding survey for seasonal picophytoplankton composition in two coral reefs around Sesoko Island, Okinawa, Japan. *J. Appl. Phycol.* **2018**, *355*, 179–3186. [[CrossRef](#)]
7. Li, J.Z.; Tao, X.; Bai, B. Geological conditions, reservoir evolution and favorable exploration directions of marine ultra-deep oil and gas in China. *Pet. Explor. Dev.* **2021**, *48*, 20. [[CrossRef](#)]

8. Campana, S.; Demey, C.; Busch, K. Marine sponges maintain stable bacterial communities between reef sites with different coral to algae cover ratios. *FEMS Microbiol. Ecol.* **2021**, *97*, fiab115. [[CrossRef](#)] [[PubMed](#)]
9. Roelfsema, C.; Kovacs, E.M.; Vercelloni, J. Fine-scale time series surveys reveal new insights into spatio-temporal trends in coral cover (2002–2018), of a coral reef on the Southern Great Barrier Reef. *Coral Reefs* **2021**, *40*, 1055–1067. [[CrossRef](#)]
10. Huang, J.S. Rock types of coral reef rocks in China. *Mar. Sci.* **1982**, *5*, 64.
11. Li, X.Y.; Lin, J.L.; Wen, H.J. Automatic recognition of carbonate pore space. *J. Daqing Pet. Inst.* **2005**, *29*, 4–6. [[CrossRef](#)]
12. Wang, J.C.; Wang, C.Y.; Zhu, C.Q.; Hu, S. Borehole image-based evaluation of coral reef porosity distribution characteristics. *Mar. Georesour. Geotechnol.* **2017**, *35*, 1008–1017. [[CrossRef](#)]
13. Wang, J.C.; Wang, C.Y. Analysis and Evaluation of Coral Reef Integrity Based on Borehole Camera Technology. *Mar. Georesour. Geotechnol.* **2017**, *35*, 26–33. [[CrossRef](#)]
14. Wang, J.C.; Chen, W.; Wang, Y.T.; Zou, J.P. Coral reef pore recognition and feature extraction based on borehole image. *Mar. Georesour. Geotechnol.* **2021**, *40*, 159–170. [[CrossRef](#)]
15. Bigerelle, M.; Iost, A. Statistical artefacts in the determination of the fractal dimension by the slit island method. *Eng. Fract. Mech.* **2004**, *71*, 1081–1105. [[CrossRef](#)]